IEEE Access
Multidisciplinary | Rapid Review | Open Access Journal

Received July 15, 2020, accepted July 25, 2020, date of publication July 29, 2020, date of current version August 12, 2020.

Digital Object Identifier 10.1109/ACCESS.2020.3012672

Tilting Path Optimization of Tilt Quad Rotor in Conversion Process Based on Ant Colony Optimization Algorithm

ZHICHAO LYU[1], ZHIGANG WANG[1], DENGYAN DUAN[2], LILI LIN[1], JIANBO LI[2], YONGWEN YANG[1], YONGHONG CHEN[1], AND YIBO LI[1]

[1]Yangzhou Collaborative Innovation Research Institute, Yangzhou 225000, China
[2]National Key Laboratory of Rotorcraft Aeromechanics, Nanjing University of Aeronautics and Astronautics, Nanjing 210016, China

Corresponding author: Zhigang Wang (wangzhigang@nuaa.edu.cn)

ABSTRACT The tilt quad rotor (TQR) has the problem of manipulation redundancy due to the aerodynamic structure changing in conversion mode. The tilting path is limited by the conversion corridor. In order to solve the problem of manipulation redundancy in conversion mode and find out the optimal tilting path in conversion corridor, the aerodynamic model of the TQR based on Goldstein vortex theory is established to obtain the manipulation derivative matrix and conversion corridor. A novel manipulation strategy is proposed, the altitude, forward velocity and tilt angle are introduced into the manipulation strategy to ensure the stability of the altitude and attitude in conversion process. To find out the optimal tilting path in conversion corridor, a novel tilting strategy is proposed based on Ant Colony Optimization (ACO) algorithm and compared with another three tilting path. To verify the credibility of the flight dynamics model, the effectiveness of manipulation strategy and tilting path optimization, the simulation and flight test were carried out. The simulation and flight test results show that the manipulation strategy proposed in this paper can solve the manipulation redundancy in conversion mode very well, and the proposed tilting path can ensure the stability of the altitude and attitude in conversion corridor.

INDEX TERMS Tilt quad rotor, manipulation strategy, ant colony optimization, tilting path, flight test.

I. INTRODUCTION

The tilt quad rotor [1]–[6] (TQR) is a novel vehicle which combines the characteristics of helicopter and fixed wing aircraft. The TQR has three flight modes: helicopter mode, fixed wing mode and conversion mode. In order to satisfy the requirements of helicopter mode and fixed wing mode, TQR has two sets of manipulation modes(helicopter and fixed wing mode), and gradually transforms with the change of nacelle tilt angle [7]–[9]. The TQR can be controlled in the same state by helicopter or fixed wing control mechanism and the tilt nacelle. Therefore, the manipulation redundancy of TQR will appear in the conversion process. In addition, the whole conversion process must be completed within the conversion corridor. How to solve the problem of manipulation redundancy is an important research topic [10]–[13].

At present, the control methods of TQR in conversion mode mainly focus on the preset control scheme to solve the problem of manipulation redundancy. The control system is designed to track the predetermined commands [14]–[17] (tilting law, flight trajectory, etc.). Oosedo *et al.* [18] present the attitude transition flight control system for pitch angles ranging 0° to 90° since flight condition with a 90° pitch angle significantly differs from that in a conventional quad rotor UAV flight, and then adequate control system and sufficient experimental validation are necessary for stable flight in a wide range of attitude conditions. Haixu *et al.* [19] reckon the body, the nacelles and the rotors to be independent entities, establishes a realistic model in the form of multi-body motion equations. In order to solve the problem of aircraft manipulating redundancy of the tilt tri-rotor UAV in the process of nacelle tilting in the transitional mode, Zhang *et al.* [20] proposed an appropriate dynamic model of the tilt tri-rotor in the transitional mode is built, and a new tilting control method based on fuzzy control. Xufeia and Renliang [21] based on the augmented flight dynamics model, the optimal landing procedure of XV-15 tilt rotor aircraft after one engine failure is formulated into a Nonlinear Optimal Control

The associate editor coordinating the review of this manuscript and approving it for publication was Xiwang Dong.

Problem, solved by collocation and numerical optimization method. Wang *et al.* [22] proposes a Negative-buoyancy Quad tilt quad rotor Autonomous Underwater Vehicle, for which an attitude-tracking controller is designed for the hover and transition modes based on a disturbance-rejection control scheme. However, they do not consider the manipulation strategy and flight trajectory of the whole tilting process under different flight missions. In fact, studying the optimal conversion process will obtain the corresponding manipulation strategy. This can not only solve the problem of manipulation redundancy, but also effectively improve the tilting efficiency. Therefore, it is necessary to study the optimal tilting path of TQR.

In the developments of optimization theory, particle swarm optimization (PSO) algorithm [23] and ant colony optimization (ACO) [24] algorithm, as new parallel optimization algorithm, have been widely used in the fields of science and engineering. Wang *et al.* [25] introduced a particle swarm optimization (PSO) and bacterial foraging optimization (BFO)-based learning strategy (PBLS) to optimize the classifier and loss function of strengthened region proposal network (SRPN), but PSO algorithm has some problems, such as premature convergence, dimension disaster and easy to fall into local extremum. Ant colony optimization (ACO) algorithm [26] is a probabilistic algorithm used to find the optimal path. This algorithm has the characteristics of distributed computation, positive feedback of information and heuristic search, and is essentially a heuristic global optimization algorithm in evolutionary algorithms [27]. The optimal tilting path problem of TQR can be reduced to a nonlinear dynamic optimal problem with state and control constrains. This problem can be solved by ant colony optimization algorithm [28]–[30]. Lu and Wang [31] proposes an event-based model which lists the events related with all phases of cooperation with partners and puts events into a dynamic supply chain network in order to understand factors that affect supply chain partnership integration. They develop a multi-objective supply chain partnership integration problem by maximizing trustworthiness, supplier service, qualified products rate and minimizing cost, and then, apply a hybrid algorithm with particle swarm optimization and ant colony optimization that aims to efficiently solve the problem. Tran *et al.* [32] adopted a swarm intelligent algorithm, Ant Colony Optimization, to solve the scheduling optimization of MRO processes with two business objectives: minimizing the total scheduling time and total tardiness of all jobs. The algorithm also has the dynamic scheduling capability which can help the scheduler to cope with the changes in the shop floor which frequently occur in the MRO processes. Oh and Lee [33] proposes a new and efficient path generation framework that considers dynamic topology changes in a complex network. Multi-directional and Parallel Ant Colony Optimization is proposed. Ant agents are divided into several groups and start at different positions in parallel. Then, gaussian process regression based pheromone update method makes the algorithm more efficient. ACO is basically applied to control parameters optimization [34]–[36]. At present, no literature has applied this method to study the optimal dynamic conversion process of TQR. For the tilt quad rotor UAV, previous researches only ensured that the tilting path was in the tilt corridor, and no one conducted optimization analysis on the tilting path in corridor. By analyzing the optimal tilting path, the tilt quad rotor can make the mode transformation faster and safer.

Therefore, in this paper, the optimal tilting path of TQR was studied on ACO method. First, the flight dynamics model of TQR was taken as the foundation. We established the dynamic model to obtain the manipulation derivative matrix and conversion corridor. Then, we proposed a novel manipulation strategy and tilting path based on ACO algorithm. Last, we designed another three tilting path to compare with the optimal tilting path. The simulation and flight test were carried out to verify the credibility of the flight dynamics model, the effectiveness of manipulation distribution strategy and tilt path optimization.

The main contributions in this manuscript are list below:

1) The aerodynamic models of propeller, wing, vertical tail and fuselage are build respectively by using the idea of component modeling [6]. The linear flight dynamic model based on the small perturbation theory is provided for the analysis of manipulation derivative and conversion corridor.
2) Based on the conversion corridor, a novel manipulation strategy is proposed. The altitude, forward velocity and tilt angle are introduced into the manipulation strategy to ensure the stability of the altitude and attitude in conversion process.
3) A novel tilting strategy is proposed based on ACO algorithm to find out the optimal tilting path in conversion corridor. To verify the manipulation strategy and optimal tilting path, the simulation of comparing with another three tilting path and flight test of principle and prototype aircraft are carried out.
4) Both the simulation and flight test results show that the manipulation strategy proposed in this paper can solve the manipulation redundancy in conversion mode very well, and the proposed tilting path can ensure the stability of the altitude and attitude in conversion corridor.

Section II shows the manipulation distribution strategy. Section III describes the tilting path optimization with ACO. Section IV shows the results and discussions of simulation and flight test. Finally, section V draws some conclusions for this paper.

II. MANIPULATION DISTRIBUTION STRATEGY

The tilt quad rotor with partial tilt wing in this paper is shown in Figure 1, including four groups of propellers, front and rear wings, fuselage, elevator, motors, tilting mechanism, undercarriage and flight control system. Both ends of the front and rear wings are designed with a tilt nacelle. The tilt wing is connected to the nacelle and turns with the tilting of

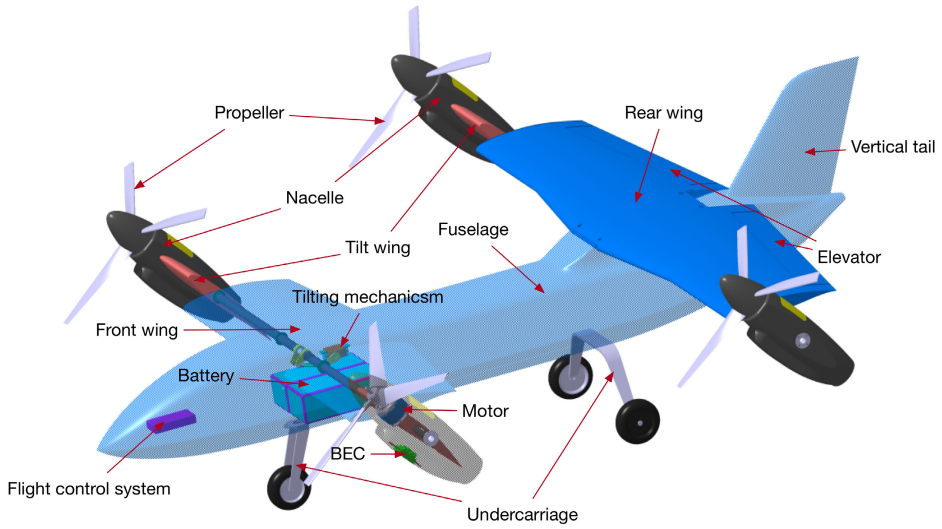

FIGURE 1. Tilt quad rotor with partial tilt wing.

TABLE 1. Parameters of the tilt quad rotor with partial tilt wing.

category	item	value	
propeller parameter	radius(inch)	20	
	Blade number	2	
	Thread pitch(inch)	12	
Wing parameter		front	rear
	Wing area(m^2)	0.28	0.475
	Tilt wing area(m^2)	0.0425(one side)	
	wingspan(m)	1.3	1.8
	Taper ratio	1.2	1.5
	Mean-chord(m)	0.265	0.3
	Aspect ratio	4.9	6
	Airfoil profile	Eppler1200	
Fuseladge parameter	length(m)	1.8	
	Maximum cross-sectional area (m^2)	0.06	
Relative position parameter	Vertical distance of front and rear wings (m)	0.08	
	Vertical distance of the two propellers on the same side(m)	0.08	
	Horizontal distance of the two propellers on the same side(m)	0.26	

the propeller in the nacelle. The parameters of the tilt quad rotor with partial tilt wing is shown in Table 1.

The tilt quad rotor has problem of manipulation redundancy in conversion process. In this section, we analysis the dynamic model of tilt quad rotor to obtain the conversion corridor and propose the manipulation strategy.

A. MANIPULATION DERIVATIVE

$$\begin{cases} F_x = m(\dot{u} + qw - rv) + mg\sin\theta \\ F_y = m(\dot{v} + ru - pw) - mg\cos\theta\sin\phi \\ F_z = m(\dot{w} + pv - qu) - mg\cos\theta\cos\phi \\ M_x = I_{xx}\dot{p} - (I_{yy} - I_{zz})qr + I_{yz}(r^2 - q^2) \\ -I_{xz}(pq + \dot{r}) + I_{xy}(pr - \dot{q}) \\ M_y = I_{yy}\dot{q} - (I_{zz} - I_{xx})pr + I_{xz}(p^2 - r^2) \\ -I_{xy}(qr - \dot{p}) + I_{yz}(pq - \dot{r}) \\ M_z = I_{zz}\dot{r} - (I_{xx} - I_{yy})pq + I_{xy}(q^2 - p^2) \\ -I_{yz}(pr - \dot{q}) + I_{xz}(qr - \dot{p}) \end{cases} \tag{1}$$

$$\begin{cases} p = \dot{\phi} - \dot{\psi}\sin\theta \\ q = \dot{\theta}\cos\phi + \dot{\psi}\sin\phi\cos\theta \\ r = -\dot{\theta}\sin\phi + \dot{\psi}\cos\phi\cos\theta \end{cases} \tag{2}$$

The dynamic equation is shown in equation (1), and the kinematics equation is shown in equation (2). Where, m is the weight of aircraft, I is the inertia matrix, u, v, w is the velocity, ϕ, θ, ψ is the euler angle, p, q, r is the angular velocity.

Nonlinear dynamic model of equation (1) and equation (2) can be described as:

$$\dot{X} = f\,(X, U, t) \tag{3}$$

where, $X = [\,u\ v\ w\ p\ q\ r\ \varphi\ \vartheta\ \psi\,]$ is system state variable. U is system control variable, which includes throttle manipulation δ_T, longitudinal manipulation δ_E, lateral manipulation δ_A, course manipulation δ_R and tilt angle β_m.

$$U = \left[\,\delta_T \quad \delta_E \quad \delta_A \quad \delta_R \quad \beta_m\,\right] \tag{4}$$

The Taylor series expansion of equation(3) is carried out at the equilibrium point. Keep the linear part and ignore the

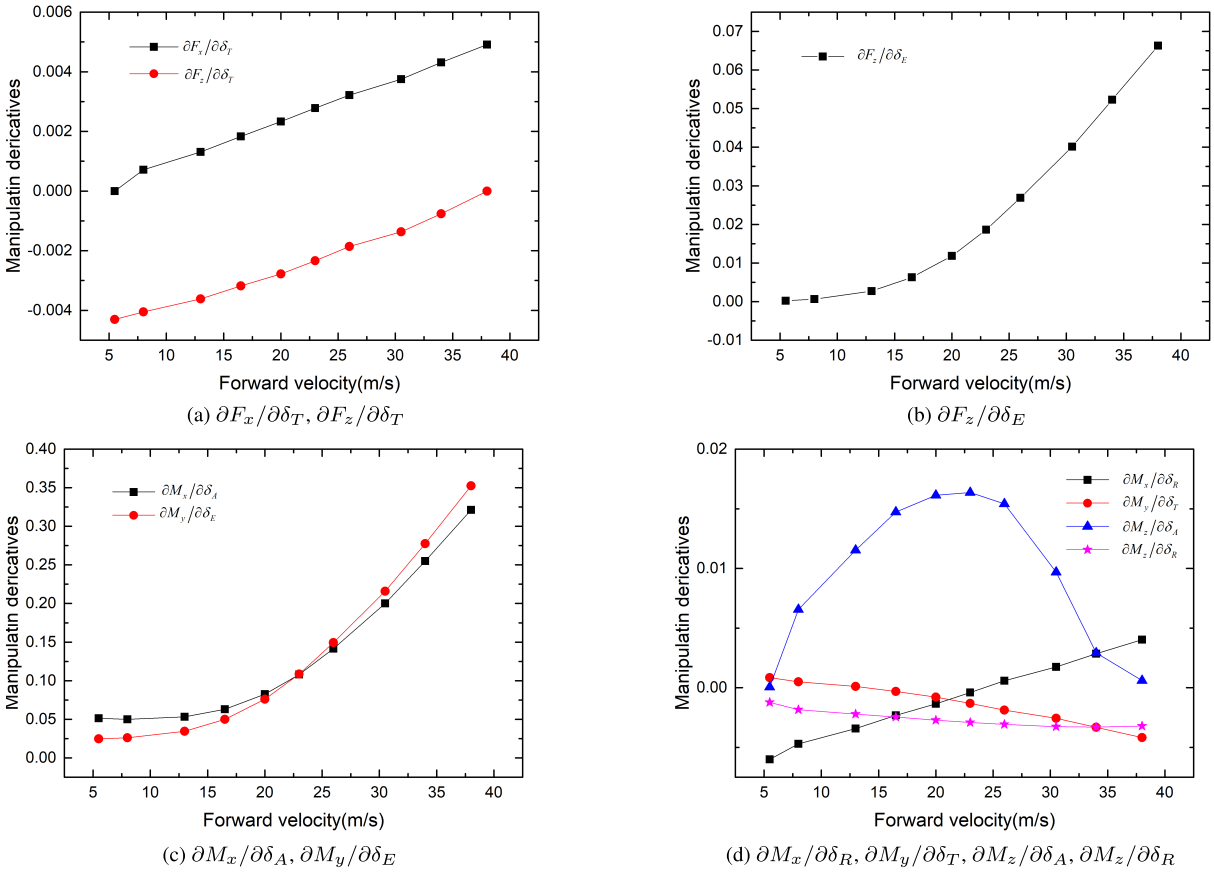

(a) $\partial F_x/\partial\delta_T, \partial F_z/\partial\delta_T$ (b) $\partial F_z/\partial\delta_E$

(c) $\partial M_x/\partial\delta_A, \partial M_y/\partial\delta_E$ (d) $\partial M_x/\partial\delta_R, \partial M_y/\partial\delta_T, \partial M_z/\partial\delta_A, \partial M_z/\partial\delta_R$

FIGURE 2. Curves of manipulation derivatives.

higher order part, one can obtain:

$$\Delta\dot{X} = \frac{\partial f}{\partial X}|X_{trim}\Delta X + \frac{\partial f}{\partial U}|U_{trim}\Delta U \tag{5}$$

where, the subscript *trim* indicates the trimming value, ΔX and ΔU are the increments of system state variables and system control variables. equation(5) can be rewritten as:

$$\Delta\dot{X} = A\Delta X + B\Delta U \tag{6}$$

where, A is system state matrix; B is control matrix.

Figure2 shows the curves of manipulation derivatives with forward velocity in conversion mode. It can be seen from Figure2 (a), (b) and (c) that with the increase of forward velocity, the manipulation derivatives of δ_T, δ_E and δ_A are enhanced. Manipulation derivatives of $\partial F_x/\partial\delta_T$ and $\partial F_z/\partial\delta_T$ are essentially linear. However, the manipulation derivatives of $\partial F_z/\partial\delta_E$, $\partial M_x/\partial\delta_A$ and $\partial M_y/\partial\delta_E$ have obvious non-monotonicity. For vertical position control, δ_T and δ_E are redundant. With the increase of β_m, the manipulation derivatives of δ_T decrease and the manipulation derivatives of δ_E increase. From Figure2 (d), we can know that with the increase of forward velocity, the manipulation derivative of $\partial M_x/\partial\delta_R$ increase, but the manipulation derivatives of $\partial M_y/\partial\delta_T$ and $\partial M_z/\partial\delta_R$ decrease. The manipulation derivative of $\partial M_z/\partial\delta_A$ increase and then decrease with the increase of forward velocity. From Figure2 (c) and (d), we can see that in the conversion mode, δ_T and δ_E have manipulation redundancy for pitch. The manipulation derivatives of δ_E is enhanced with the increase of forward velocity, while the manipulation derivatives of δ_T is receded. The lateral and course have coupling manipulations. The effect of δ_A on course coupling is greater than that of δ_R on lateral coupling. Especially, the manipulation derivatives of δ_A on course is enhanced with the tilt angel β_m increase at beginning, however, when the tilt angle reached a certain value, the manipulation derivatives of δ_A on course is receded. Therefor we can know from Figure 2 the forward velocity and tilt angle β_m have great influence on the manipulation derivatives.

B. MANIPULATION STRATEGY

The maximum and minimum velocity under each tilt angle are calculated, and then the conversion corridor of TQR with partial tilt wing are obtained. The minimum velocity boundary is mainly determined by whether the wing reaches the stall angle of attack, and the maximum velocity boundary is mainly determined by whether the propeller power reaches the maximum power.

Figure 3 shows the conversion corridor of the tilt quad rotor with partial tilt wing. When the tilt angle is 90°, the aircraft

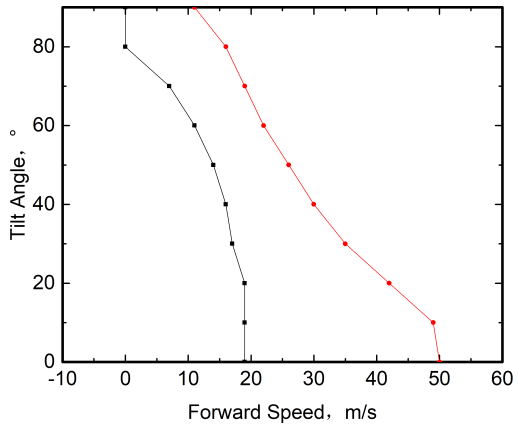

FIGURE 3. Tilt transition corridor.

is helicopter mode; when the tilt angle is 0°, the aircraft is fixed-wing mode. The black line is the boundary of minimum velocity of the TQR with partial tilt wing. The red line is the boundary of maximum velocity of TQR with partial tilt wing.

The aircraft conversion process is a variable velocity and structure process which must reasonably control the aerodynamic distribution between propeller and wing. If the forward velocity is too small that will lead to the wing stalled. Therefore, the conversion mode is a process about altitude, forward velocity and tilt angle. The change of tilt angle β_m of nacelle is as follows:

$$\beta_m = \omega_\beta \cdot t \tag{7}$$

where, ω_β is tilt velocity based on altitude and forward velocity and t is tilt time.

In the conversion mode, the TQR always maintains the attitude angle and altitude stability to achieve a safety conversion flight. In terms of altitude manipulation, it is necessary to automatically compensate the propeller rotational speed and the elevator to achieve altitude stability. The altitude control and manipulation strategy used in the TQR is shown in figure 4.

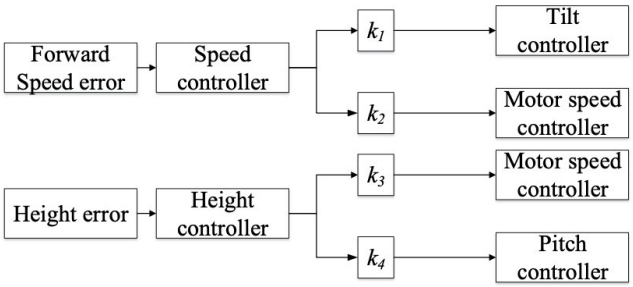

FIGURE 4. Manipulation distribution in transition mode.

Where, k_1, k_2, k_3, k_4 are distribution coefficient related to the tilt angle β_m and forward velocity in figure 3.

$$k_1 = \left(\left(\cos\left(2\left(\pi/2 - \beta_m\right)\right)\right) + 1\right)/2 \tag{8}$$

$$k_2 = \left(\left(\sin\left(2\left(\pi/2 - \beta_m\right) - \pi/2\right)\right) + 1\right)/2 \tag{9}$$

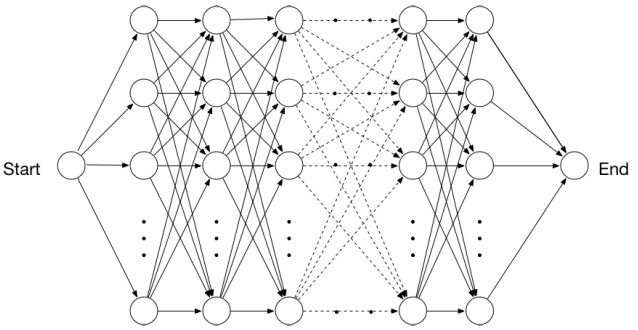

FIGURE 5. ACO optimization graph.

$$k_3 = \begin{cases} 1 & u < 18 \\ 1 - \dfrac{u - 18}{20} & 18 \le u < 38 \\ 0 & u \ge 38 \end{cases} \tag{10}$$

$$k_4 = \begin{cases} 0 & u < 18 \\ \dfrac{u - 18}{20} & 18 \le u < 38 \\ 1 & u \ge 38 \end{cases} \tag{11}$$

where, $u = 18$ is the minimum forward velocity of the TQR in fixed wing mode and $u = 38$ is the maximum forward velocity of the TQR in conversion mode ($\beta_m = 60°$).

III. TILTING PATH OPTIMIZATION

A. THEORY OF ANT COLONY OPTIMIZATION

ACO is a meta-heuristic algorithm based on the foraging behavior of ants, which can be simplified as finding an optimal path in the optimization graph composed of nodes. Therefore, the basic idea of ACO is: the ant's walking path in the optimization graph is used to represent the feasible solution of the optimization problem. All the paths in the optimization graph constitute all feasible solutions of optimization problem. ACO is to find the optimal solution of optimization problem from all the feasible solutions of optimization problem.

At the beginning, put m ants randomly into n nodes, meanwhile, the first element of each ant's tabu table is set to its current node. The amounts of pheromones in each path is equal, assign $\tau_{ij}(0) = c$ (c is a small constant). Each ant independently selects the next node according to the heuristic information (the distance between two nodes) and the amount of pheromone remaining on the path. At time t, the probability that ant k moves from node i to node j is:

$$p_{ij}^k(t) = \begin{cases} \dfrac{\left[\tau_{ij}(t)\right]^\alpha \cdot \left[\eta_{ij}(t)\right]^\beta}{\sum_{s \in J_k(i)} \left[\tau_{is}(t)\right]^\alpha \cdot \left[\eta_{is}(t)\right]^\beta} & j \in J_k(i) \\ 0 & other \end{cases} \tag{12}$$

where,$J_k(i) = \{1, 2, \cdots, n\} - tabu_k$ represents the next set of nodes that ant k is allowed to select. $tabu_k$ records the nodes that ant k currently walking through. When all n nodes are added to $tabu_k$, ant k has finished a path. The path of ant k

walked is a feasible solution of optimization problem. η_{ij} in equation(12) is heuristic factor which represents the expectation of ant moving from node i to node j. α and β represent the relative importance of pheromone and heuristic factor. When all the ants have completed a journey, pheromones on each path are updated according to equation(13):

$$\tau_{ij}(t+n) = (1-\rho)\cdot\tau_{ij}(t) + \Delta\tau_{ij} \tag{13}$$

where:ρ $(0 < \rho < 1)$ is the evaporation coefficient of the pheromone on the path, $1-\rho$ represents the persistence coefficient of pheromone; $\Delta\tau_{ij}$ represents the increment of pheromone on edge ij:

$$\Delta\tau_{ij} = \sum_{k=1}^{m} \Delta\tau_{ij}^{k} \tag{14}$$

where, $\Delta\tau_{ij}^{k}$ represents the pheromone of ant remained on the edge ij.

$$\Delta\tau_{ij}^{k} = \begin{cases} \dfrac{Q}{L_k} & \text{ant } k \text{ go through edge } ij \\ 0 & \text{other} \end{cases} \tag{15}$$

where, Q is positive constant, L_k represents the length of ant k walking path in this journey.

Algorithm 1 ACO Algorithm

Parameters initialization. Assign time $t = 0$ and number of cycles $N_c = 0$, assign maximum number of cycles G, put m ants on n elements, the initial pheromone of each edge (i, j) on a digraph $\tau_{ij}(t) = c$, where c is constant, and at beginning $\Delta\tau_{ij}(0) = 0$;
while *Termination criterion* $N_c < G$ **do**
  $N_c \longleftarrow N_c + 1$;
  Index number of ant tabu $k = 1$;
  for *each ant* $k, k \in [1, m]$ **do**
    for *each dimension,* $j \in [1, n]$ **do**
      if *the elements in set C are not traversal* **then**
        The individual ant selects element j and advances according to the probability calculated by the state transition probability equation(12), $j \in \{J_k(i)\}$;
        Modify tabu pointer, move the ant to the new element, and move the element to the tabu of the individual ant;
      else
        Record the best path;
        Update pheromones on each path according to equations(13) and(14);
output optimization result

ACO algorithm is implemented in Algorithm 1. The process diagram of ACO is shown in figure 6.

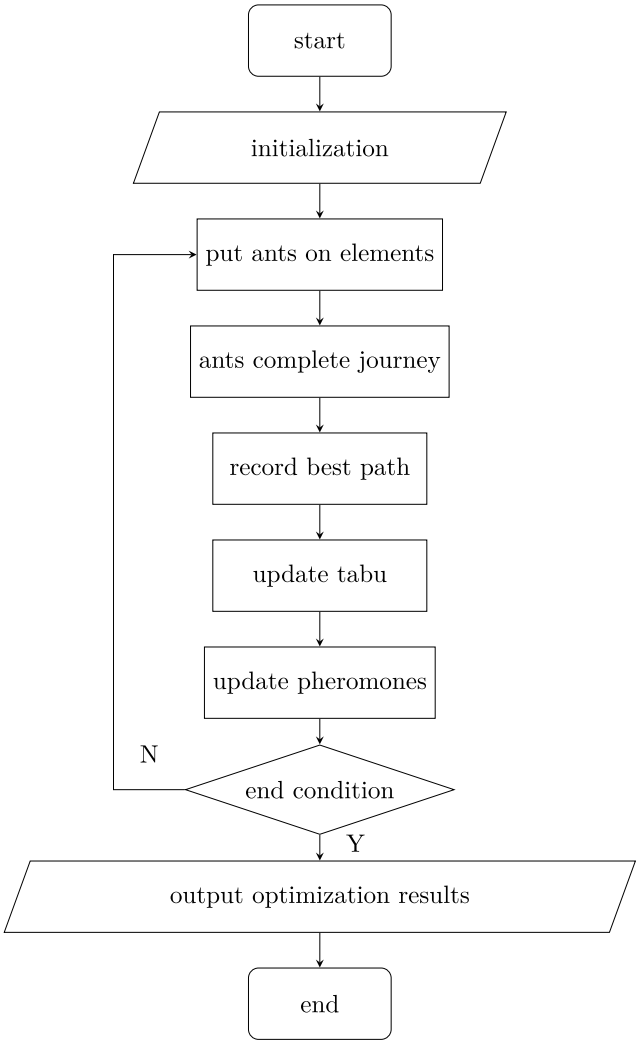

FIGURE 6. ACO process diagram.

B. BOUNDARY CONDITIONS

In the conversion process, we make the UAV complete the conversion process in the shortest time under the altitude maintenance. From subsection II.A, we can see that the change in altitude is mainly caused by δ_T, θ, u and β_m.

Tilting path optimization is to solve the nonlinear equations of equation (3):

$$g_i(X_I) = 0 \qquad (i = 1, 2, 3, 4) \tag{16}$$

Constructing the target function:

$$J = h(X_I) = Min \sum_{i=1}^{4} g_i^2(X_I) \tag{17}$$

The constraint condition of tilting path can be expressed as:

$$\begin{cases} w = 0 \\ 0 \le \delta_T \le \delta_{T\max} \\ 5^\circ \le \theta \le 14^\circ \\ u_{\min} \le u \le u_{\max} \\ 0^\circ \le \beta_m \le 90^\circ \end{cases} \tag{18}$$

where, the maximum value of θ is the stall angle of attack in the conversion mode, and the minimum value of θ is to ensure that the TQR always fly at a positive angle of attack. u_{min} and u_{max} are the left and right boundary of corridor in figure 3. By using the conversion corridor to determine the constraints, the dynamic conversion process can be kept in the conversion corridor.

C. OPTIMIZATION RESULTS

In order to obtain the best performance for ACO, its userdefined parameters are worth investigating. There are seven key parameters in ACO, i.e., the number of ants(m); the transfer probability(P); the evaporation coefficient of the pheromone(ρ); the maximum number of iterations(G). It is obvious that G remarkably influences the computational time of ACO.

In this experiment, the Taguchi's method [37] is used to acquire a reasonable combination of seven ACO parameters. The number of levels for four factors are set as follows: three levels for $m \in \{10, 20, 30\}$; three levels for $P \in \{0.1, 0.2, 0.3\}$; three levels for $\rho \in \{0.2, 0.5, 0.9\}$; and three levels for $G \in \{1500, 2000, 2500\}$. A full factorial analysis needs $3^4 = 81$ experiments. Compared with the full factorial analysis, Taguchi's method adopts the orthogonal arrays so as to decrease greatly the number of experimental runs, the cost of time, manpower, and materials. Therefore, an orthogonal array $L_9(3^4)$ that contains only 9 experiments is adopted in our experiment. The level values of each key parameter are shown in the table2.

TABLE 2. Level values of each key parameter.

parameter	symbol	1	2	3
m	A	10	20	30
P	B	0.1	0.2	0.3
ρ	C	0.2	0.5	0.9
G	D	1500	2000	2500

According to Taguchi's test method, four key parameters of the number of ants(m); the transfer probability(P); the evaporation coefficient of the pheromone(ρ); the maximum number of iterations(G) were analyzed sensitively. The calculation results are shown in Table 2, where, Delta is the difference between the maximum average response value and the minimum average response value for each factor, and the rank is assigned based on the Delta value. Rank 1 is assigned to the largest Delta, rank 2 to the second largest Delta, and so on, to represent the relative effect of each factor on the response.

In Taguchi's experiments, we want to make the standard deviation as small as possible and the SNR and slope as large as possible among all the results. It can be seen from the SNR results in table 3 that the ρ (Delta $= 14.42$, rank $= 1$) has the greatest effect on the SNR, followed by G (Delta $=$ 12.55, rank $= 2$), and then the m and P. It can be seen from the mean value results in table 4 that the ρ (Delta $=$ 0.002657, rank $= 1$) has the greatest effect on the mean

TABLE 3. Response of SNR (Signal to Noise Ratio).

level	m	P	ρ	G
1	55.44	55.10	50.78	50.82
2	52.46	57.96	54.79	56.56
3	62.86	57.70	65.20	63.37
Delta	10.41	2.86	14.42	12.55
Rank	3	4	1	2

TABLE 4. Response of mean value.

level	m	P	ρ	G
1	0.002542	0.002599	0.003247	0.002870
2	0.001992	0.001064	0.001441	0.001658
3	0.000745	0.001616	0.000590	0.000751
Delta	0.001797	0.001534	0.002657	0.002119
Rank	3	4	1	2

TABLE 5. Response of standard deviation value.

level	m	P	ρ	G
1	0.002856	0.002692	0.003607	0.003032
2	0.001984	0.001043	0.001241	0.001805
3	0.000541	0.001646	0.000533	0.000545
Delta	0.002315	0.001649	0.003074	0.002487
Rank	3	4	1	2

value, followed by G (Delta $= 0.002119$, rank $= 2$), and then the m and P. It can be seen from the standard deviation value results in table 5 that the ρ (Delta $= 0.003074$, rank $= 1$) has the greatest effect on the standard deviation value, followed by G (Delta $= 0.002487$, rank $= 2$), and then the m and P.

In the simulation analysis of ACO algorithm, we found that although ACO algorithm has the advantages of distributed parallel mechanism, easy to combine with other algorithms and robustness, it has the prominent disadvantages such as long search time and easy to fall into local optimum. Its complexity reflects this phenomenon, the time complexity is $O(n^4)$ and the space complexity is $O(n^2)$. Moreover, this method is prone to stagnation, that is, after searching to a certain extent, the solutions found by all individuals are exactly the same, and the further searching of solution space is not conducive to finding better solutions.

Through the simulation analysis of the key parameters of ACO algorithm, the main parameters of ACO are determined as shown in the table 6.

TABLE 6. Selfdefined parameters of ACO algorithm.

parameter	value	description
m	20	Number of ants
P	0.2	Transfer probability constant
ρ	0.2	Evaporation coefficient of the pheromone
G	2000	Maximum number of iterations

Figure 7 shows the curves of optimization result with different tilt angle. We can see that ACO convergence very quickly. At the beginning of the conversion process, the variation of throttle is larger, it is due to the vertical manipulation

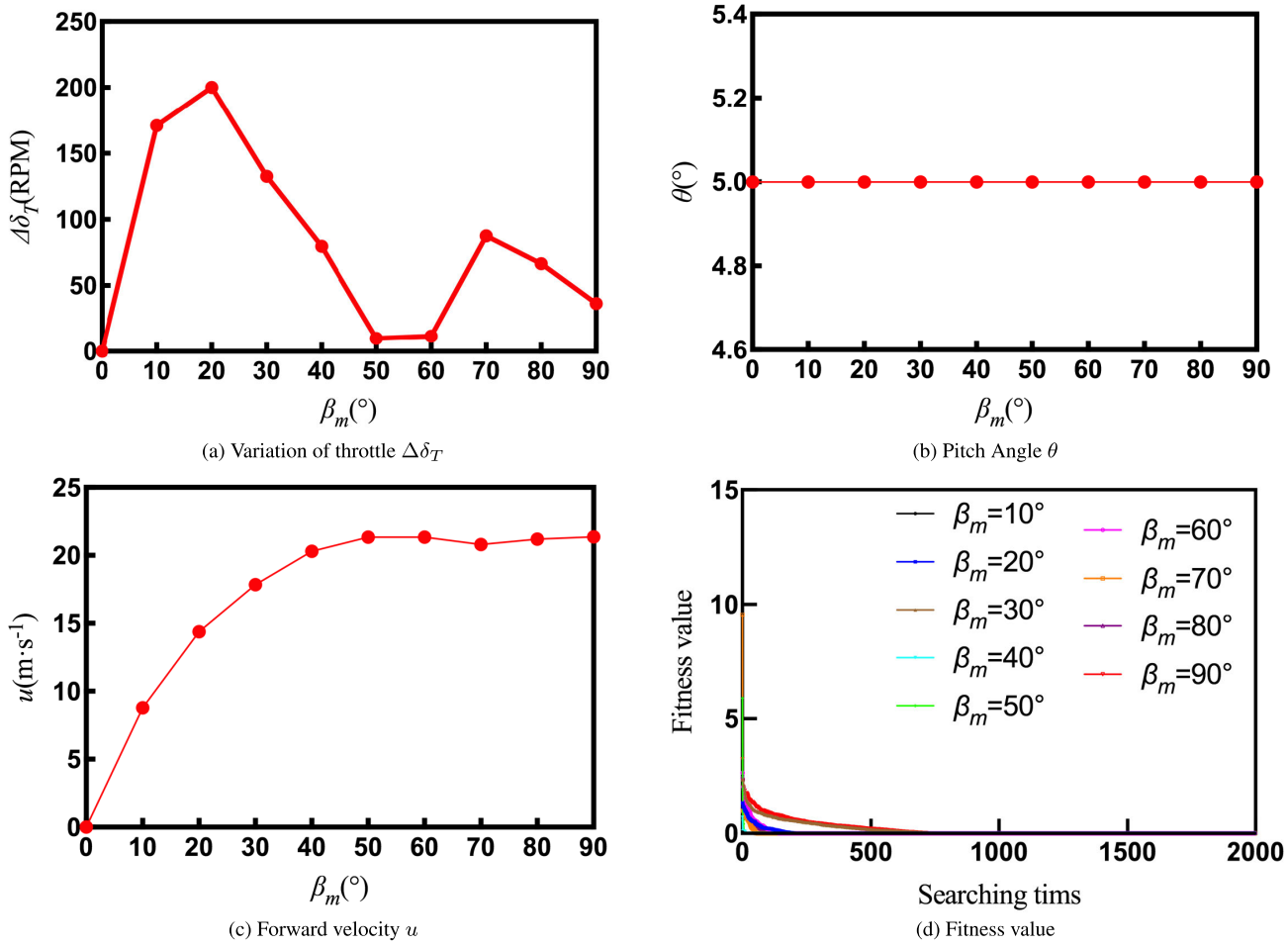

(a) Variation of throttle $\Delta\delta_T$

(b) Pitch Angle θ

(c) Forward velocity u

(d) Fitness value

FIGURE 7. Optimization result with different tilt angle β_m.

is mainly based on throttle. The change of throttle decreases with the increase of tilt angle. When the tilt angle is larger than 60°, due to the increase of forward velocity, the variation of elevator plays a major role. This is consistent with the analysis of manipulation strategy in subsection II.A. During the entire conversion process, the pitch angle of TQR can be a positive angle 5°. The required forward velocity increase with the increase of tilt angle. However, when the tilt angle is above 50°, the required forward velocity is basically the same. It is because the lift provide by the wings can balance gravity perfectly. The tilt rate of the tilt angle can be set to a multi-stage mode by means of the change trend of required forward velocity. In order to speed up the conversion process that is to shorten the conversion time, we can rewrite equation (7) as:

$$\beta_m = \begin{cases} 10t_1 & 0° \le \beta_m \le 30° \\ 20t_2 + 10t_1 & 30° < \beta_m \le 50° \\ 40t_3 + 20t_2 + 10t_1 & 50° < \beta_m \le 90° \end{cases} \quad (19)$$

where, t_i $(i = 1, 2, 3)$ is tilt time.

TABLE 7. Parameters of the four conditions.

	Condition1	Condition2	Condition3	Condition4
Tilt rate 1(°/s)	10	10	10	10
Tilt rate 2(°/s)	20	20	10	10
Tilt rate 3(°/s)	40	40	10	10
Set speed 1(m/s)	17.9[1]	–	19.9	–
Set speed 2(m/s)	20[2]	–	20	–
Set tilt angle 1(°)	30	–	30	–
Set tilt angle 2(°)	50	–	50	–

[1],[2] values are set according to figure 7(c)

IV. RESULT AND DISCUSSION

A series of simulation and flight test are carried out to verify the manipulation strategy and tilting path.

A. SIMULATION

Manipulation distribution strategy is designed according to subsection II.B. Tilting strategy is designed according to section III. In order to compare the tilting path optimization strategy, we designed another three conversion strategies. The conversion parameters of the four conditions are shown in table 7.

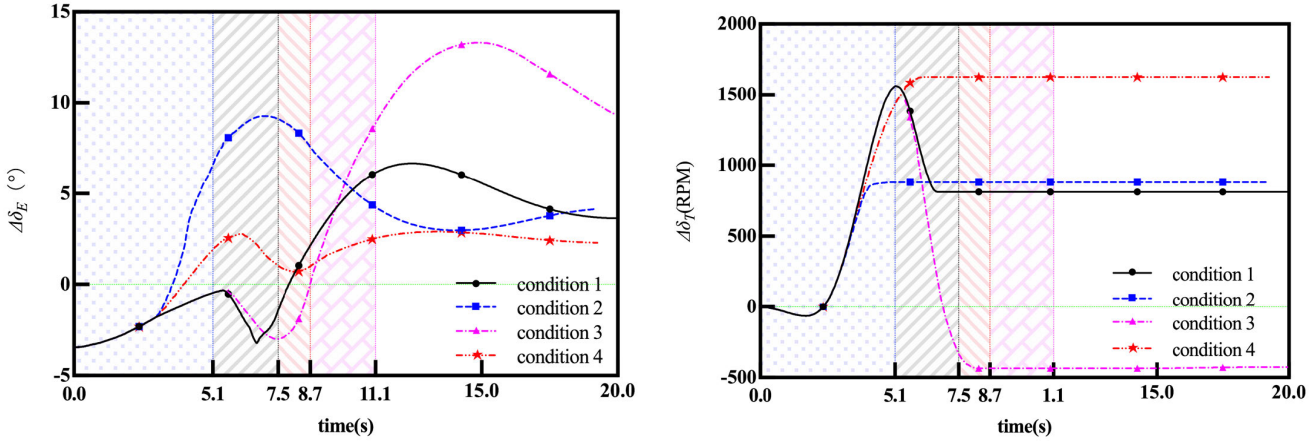

(a) Manipulation distribution δ_E

(b) Manipulation distribution δ_T

FIGURE 8. **Manipulation curves of flight simulation results.**

- **Condition 1:** conversion with different tilt rate, and waiting for the forward velocity to reach the set speed at the set tilt angle (optimal tilting path in section III);
- **Condition 2:** directly conversion from helicopter mode to fixed wing mode at different tilt rate;
- **Condition 3:** conversion with one tilt rate, and waiting for the forward velocity to reach the set speed at the set tilt angle;
- **Condition 4:** directly conversion from helicopter mode to fixed wing mode at one tilt rate.

Figure 8 and 9 shows the results of flight simulation. The shaded parts represent the conversion process of the four conditions. From figure 9 we can see that at the beginning of conversion, the forward velocitys are same in all four conditions. But with the tilt angle increases, the increment of forward velocity changes gradually. When the tilting process finished, the forward velocity of the four condition 1-4 are 24m/s, 20m/s, 22m/s and 30m/s. At the beginning, the altitudes are same in all four conditions, and then the altitudes of condition 1,3 and 4 increase but the altitude of condition 2 is continue to decrease. The minimum altitudes of the four conditions in conversion process are -1.3m, -3.1m, -5.5m and -1.6m. When the QTR turn to the fixed wing mode, the altitudes of the four conditions change to 1.3m, -3.1m, -5.5m and 0.9m. Same as altitude and forward velocity, the pitch angles are the same at the beginning. The pitch angles of the four conditions are $-3.0°$, $4.5°$, $0.4°$ and $8.3°$. When the tilt angle is less than $30°$, the tilt rate is same, so when tilt time is 3s, the nacelle tilt angles are all $30°$ in the four conditions. When the tilt angle is above $30°$, the nacelles continue tilting. However, the tilt angles of condition 2 and 4 are unchanged because of the forward velocity. And it waits about 2.4s for the forward velocity reaching the set speed at tile angle $30°$. In these four conditions, the time spent in the tilting process is about 5.1s, 7.5s, 8.7s and 11.1s.

We can see from the results of flight simulation (Figure9) that in the first stage of conversion process ($\beta_m < 30°$). the simulation results are same due to the same of the constraint conditions of the four conditions. The forward velocity is established slowly, hence, the TQR lowers its head to speed up the forward velocity according to manipulation strategy. Then, it leads to a reduction in altitude. When $30° \leq \beta_m < 50°$, for condition 2 and condition 4, the nacelle continue tilting, while the nacelle of condition 1 and condition 3 waits the forward velocity establishing at $\beta_m = 30°$. Due to the tilt rate of condition 2 is much faster than condition 4, the forward velocity in condition 2 is increasing faster than the speed in condition4 and the vertical tension in condition 2 provided by the propellers is sharply reduced. The increased lift provided by the wing is not enough to balance the reduced vertical tension of the propeller, so the altitude is reduced sharply. It will lead the pitch angle in condition 2 is bigger than that in condition 4 to reduce the change of altitude according to manipulation strategy in subsection II.B. When the forward velocity reaches the set speed at $\beta_m = 30°$, the results of flight simulation in condition 1 and condition 3 are same to the results in condition 2 and 4. In the conversion process, the change of altitude is crucial to the safety of the conversion flight. The increase in altitude can be regarded as a safe state of flight. From all of the four flight conditions, we can see that the minimum altitudes of the four flight conditions are -1.3m, -3.1m, -5.5m and -1.6m. condition 1 is our most desired flight condition. The conversion time is shorter (7.5s). The pitch angle changes more smoothly, and the whole conversion process is much faster and more stable.

Figure 10 shows the tilting path of different conditions in conversion corridor. From the figure we can see that the tilting strategy of condition 2 is all out of the conversion corridor. The condition 4 is better than condition 1, but worse than condition 1 and condition 3. The tilting strategy of

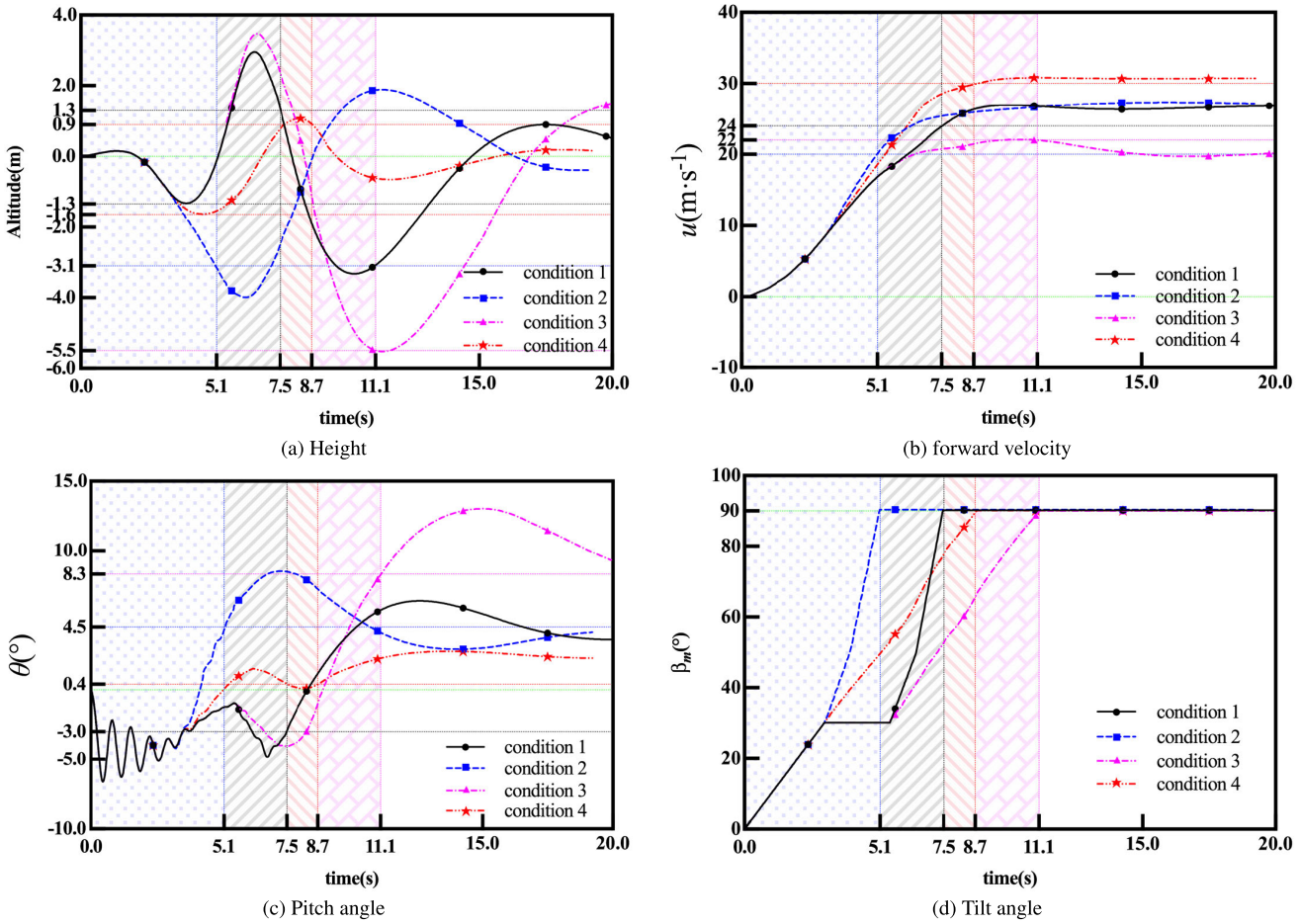

FIGURE 9. State curves of flight simulation results.

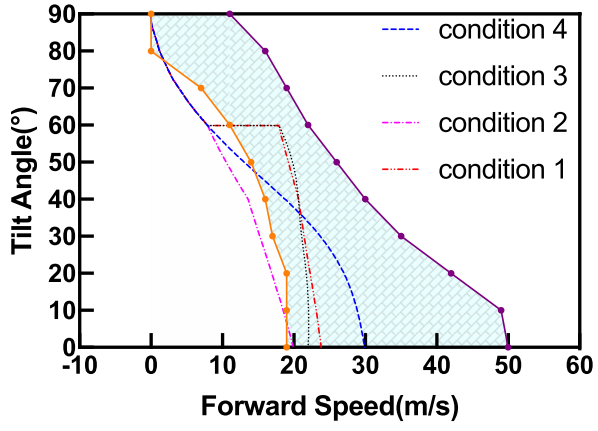

FIGURE 10. Tilting path of different conditions in conversion corridor.

condition 1 and condition 3 are similar in the conversion corridor. However, compared with figure 9 we can know that the change of altitude and pitch angle of condition 1 is smaller than that of condition 3.

From the simulation results, it can be seen that the tilting strategy proposed in this paper is reasonable and effective, which can ensure the stability of the height and attitude of the aircraft in the conversion process.

B. FLIGHT TEST

The UAV has a quick-release structure for easy transportation. Figure 11 shows several key states of the principle aircraft during the flight test. Figure 12 is the hover flight test of the prototype aircraft. Figure 13 shows several key states of the prototype aircraft during the flight test. Figure 16 is partial flight path in the whole flight test.

In helicopter mode, the UAV can maintain good stability and be sensitive to control. The acceleration process of the UAV is relatively obvious through the tilt of the nacelle and the acceleration is relatively fast. During the conversion, the nacelle began to tilt forward and the forward velocity increased rapidly. When the current flight speed reaches 18m/s, the nacelle will continue to tilt to the horizontal position to complete the mode change and switch to the fixed-wing mode. Under the fixed-wing mode cruise flight,

(a) hover (b) conversion (c) cruise

FIGURE 11. Principle aircraft flight mode.

FIGURE 12. Hover flight test.

(a) hover (b) conversion (c) cruise

FIGURE 13. Prototype aircraft flight mode.

the unmanned vehicle can quickly follow the control of the remote control to conduct a stable stability control flight.

The flight test results of forward conversion process are shown in figure 14(a) – (c). Figure 14(d) – (f) show the flight test results of the tilt quad rotor in backward conversion process. As we can see from figure14(a), in the forward conversion process, we do not give the pitch command signal. The tilt quad rotor will change the pitch angle based on the manipulation strategy to ensure the stability of the altitude(figure 14(c)). The range of pitch angle in forward conversion process is about 8°. From figure14(b), we can know that at the beginning of the forward conversion process, the increase of the forward velocity is slowly. While with the forward conversion process goes on, the forward velocity can increase rapidly. The tilt quad rotor in backward conversion process can be controlled as helicopter, which is different from the forward conversion process. When the flight mode changing from fixed wing mode to helicopter mode, the tilt quad rotor will tilt its nacelle from the horizontal position to the vertical position. Figure 15 shows the tilting path of prototype aircraft in the conversion corridor. From the figure we can see that the tilting path is similar to the proposed manipulation strategy.

The flight tests verify the reasonable and effective of manipulation strategy and tilting path optimization proposed in this paper.

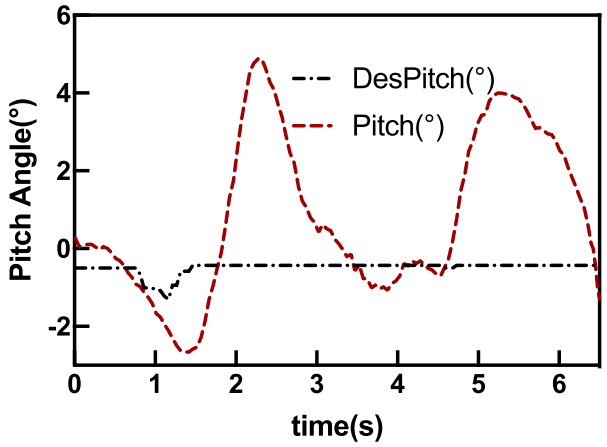

(a) Attitude in forward conversion

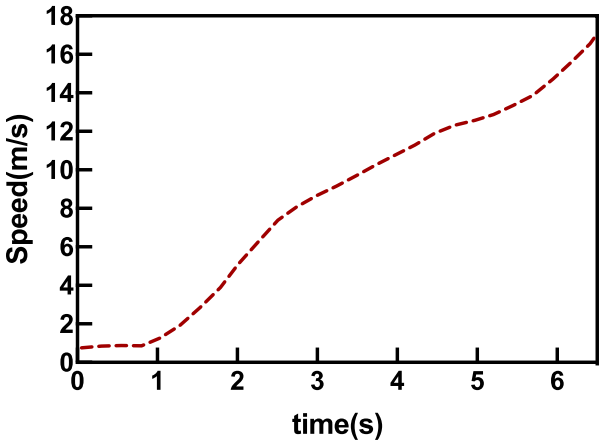

(b) Speed in forward conversion

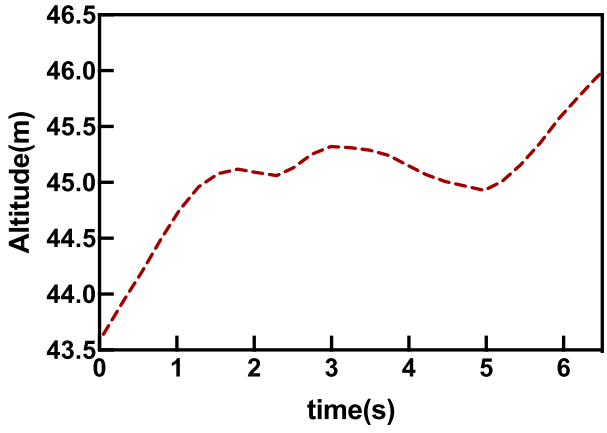

(c) Altitude in forward conversion

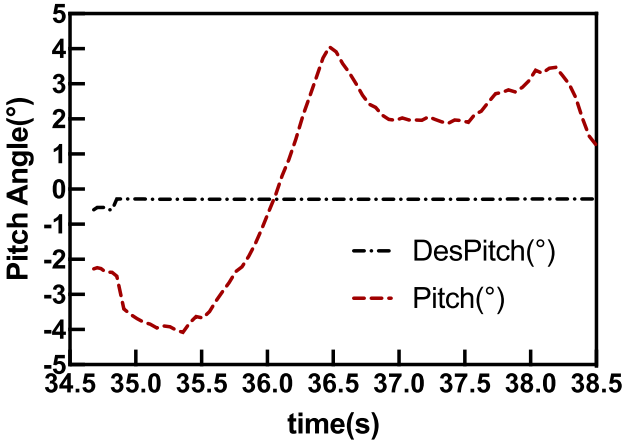

(d) Attitude in backward conversion

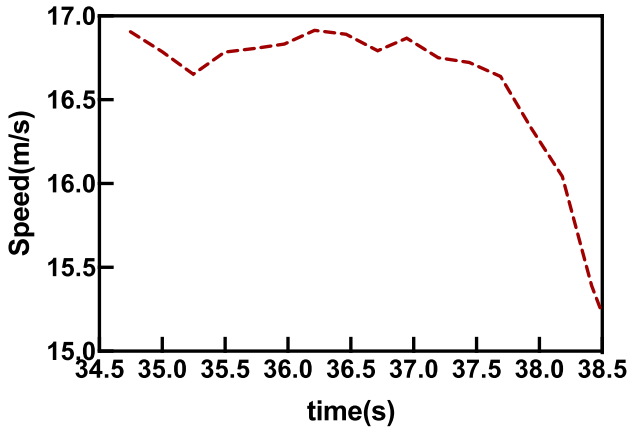

(e) Speed in backward conversion

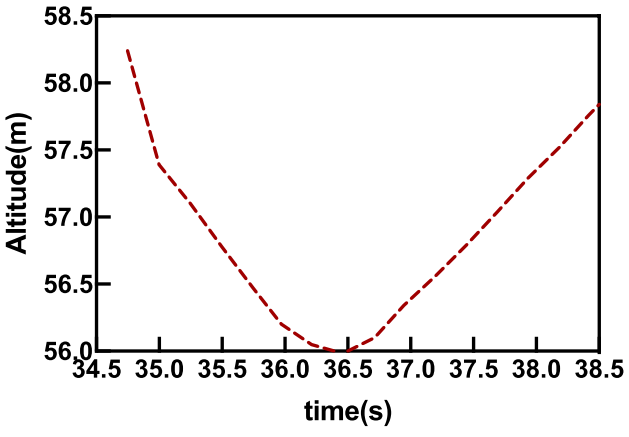

(f) Altitude in backward conversion

FIGURE 14. Flight results.

C. ANALYSIS

From subsection SIMULATION and FLIGHT TEST, we can know that the tilting strategy of condition 1 is much better than others. Based on ACO optimized tilting strategy, the aircraft can maintain relatively stable altitude and attitude during the entire tilting transition. At the initial conversion stage, the forward flight speed of the aircraft is small and the flight speed is established slowly, which is determined by the manipulation strategy in subsection II.B. Due to the small forward flying speed, the lift force provided by the wings is not enough to offset the gravity of the aircraft. At this time, the main control mode of the aircraft is helicopter mode.

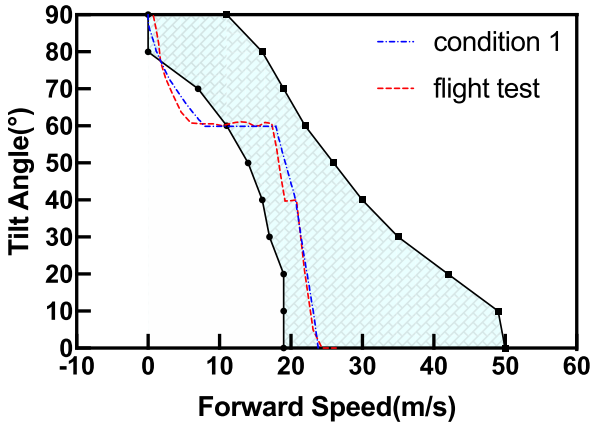

FIGURE 15. Tilting path in conversion corridor.

FIGURE 16. Partial flight path.

In order to increase the forward flying speed of the aircraft while maintaining a stable altitude, the tilt nacelle is tilted forward slowly. As the forward tilt angle of the tilt nacelle increases, the forward flight speed of the aircraft increases, and the lift force provided by the wing can gradually offset the gravity. The control mode of the aircraft gradually changes to the fixed-wing mode. The tilt nacelle quickly tilts to a horizontal position to complete the mode conversion. In the whole process of tilting, the tilting path of the aircraft is basically in the tilt conversion corridor. This proves that the manipulation strategy and tilting path optimization strategy proposed in this paper are effective and feasible.

V. CONCLUSION

In this paper, the TQR has the problem of aerodynamic structure changing in conversion mode. In order to solve the manipulation redundancy and find out the optimal tilting path in conversion corridor, The aerodynamic model of the tilt quad rotor based on Goldstein vortex theory is established to obtain the manipulation derivative matrix and conversion corridor. A novel manipulation strategy based on the analysis of manipulation derivative matrix and conversion corridor is carried out to solve the manipulation redundancy problem. A novel tilting path based on ACO algorithm is proposed and compared with another three tilting path. The simulation and flight test results show that the manipulation strategy proposed in this paper can solve the manipulation redundancy in conversion mode very well, and the proposed tilting path can ensure the stability of the altitude and attitude in conversion corridor.

ACKNOWLEDGMENT

The authors would like to thank all those who have helped during the writing of this article. They also thank the help of Prof. Jianbo Li. They appreciate his patience, encouragement, and professional instructions during the writing of this article.

REFERENCES

[1] G. R. Flores, J. Escareño, R. Lozano, and S. Salazar, "Quad-tilting rotor convertible MAV: Modeling and real-time hover flight control," *J. Intell. Robot. Syst.*, vol. 65, nos. 1–4, pp. 457–471, Jan. 2012.

[2] M. Hassanalian, R. Salazar, and A. Abdelkefi, "Conceptual design and optimization of a tilt-rotor micro air vehicle," *Chin. J. Aeronaut.*, vol. 32, no. 2, pp. 369–381, Feb. 2019.

[3] Z. Wang and J. Li, "3D simulation of flight control system for quad tilt rotor UAV based on flightgear," in *Proc. IOP Conf. Ser. Earth Environ. Sci.*, vol. 440, 2020, Art. no. 052056.

[4] Z. Wang, R. Zu, D. Duan, and J. Li, "Tuning of ADRC for QTR in transition process based on NBPO hybrid algorithm," *IEEE Access*, vol. 7, no. 1, pp. 177219–177240, 2019.

[5] Z. Wang, J. Li, and D. Duan, "Manipulation strategy of tilt quad rotor based on active disturbance rejection control," *Proc. Inst. Mech. Eng., G, J. Aerosp. Eng.*, vol. 234, no. 3, pp. 573–584, 2020.

[6] Z. G. Wang, D. Y. Duan, Y. W. Yang, H. R. Yu, and J. B. Li, "Analysis of flight dynamics characteristics of tilt quad rotor with partial tilt-wing," *Trans. Nanjing Univ. Aeronaut. Astronaut.*, vol. 36, no. 6, pp. 938–951, 2019.

[7] C. Papachristos, K. Alexis, and A. Tzes, "Hybrid model predictive flight mode conversion control of unmanned quad-TiltRotors," in *Proc. Eur. Control Conf. (ECC)*, Jul. 2013, pp. 1793–1798.

[8] Z. Wang and J. Li, "A novel active disturbance rejection control for the quad tilt rotor in conversion process," in *Proc. IOP Conf. Ser. Earth Environ. Sci.*, vol. 440, 2020, Art. no. 032036.

[9] Z. Wang, H. Zhao, D. Duan, Y. Jiao, and J. Li, "Application of improved active disturbance rejection control algorithm in tilt quad rotor," *Chin. J. Aeronaut.*, vol. 33, no. 6, pp. 1–23, 2020.

[10] C.-J. Kim, S. Sung, S. H. Park, S. N. Jung, and T. S. Park, "Numerical time-scale separation for rotorcraft nonlinear optimal control analyses," *J. Guid., Control, Dyn.*, vol. 37, no. 2, pp. 658–673, Mar. 2014.

[11] C. L. Bottasso, A. Croce, D. Leonello, and L. Riviello, "Optimization of critical trajectories for rotorcraft vehicles," *J. Amer. Helicopter Soc.*, vol. 50, no. 2, pp. 165–177, Apr. 2005.

[12] D. Chao, B. Huihui, and Z. Jianping, "Nonlinear stabilization control of tilt rotor UAV during transition flight based on HOSVD," in *Proc. IEEE Chin. Guid., Navigat. Control Conf.*, Aug. 2016, pp. 154–159.

[13] P. Huangzhong, Z. Ziyang, and G. Chen, "Tiltrotor aircraft attitude control in conversion mode based on optimal preview control," in *Proc. IEEE Chin. Guid., Navigat. Control Conf.*, Aug. 2014, pp. 1544–1548.

[14] E. B. Carlson and Y. J. Zhao, "Prediction of tiltrotor height-velocity diagrams using optimal control theory," *J. Aircr.*, vol. 40, no. 5, pp. 896–905, 2015.

[15] Y. Okuno and K. Kawachi, "Optimal takeoff procedures for a transport category tiltrotor," *J. Aircr.*, vol. 30, no. 3, pp. 291–292, 2014.

[16] G. Flores and R. Lozano, "Transition flight control of the quad-tilting rotor convertible MAV," in *Proc. Int. Conf. Unmanned Aircr. Syst.*, May 2013, pp. 789–794.

[17] G. R. Flores-Colunga and R. Lozano-Leal, "A nonlinear control law for hover to level flight for the quad tilt-rotor UAV," *IFAC Proc. Volumes*, vol. 47, no. 3, pp. 11055–11059, 2014.
[18] A. Oosedo, S. Abiko, S. Narasaki, A. Kuno, A. Konno, and M. Uchiyama, "Large attitude change flight of a quad tilt rotor unmanned aerial vehicle," *Adv. Robot.*, vol. 30, no. 5, pp. 326–337, Mar. 2016.
[19] L. Haixu, Q. Xiangju, and W. Weijun, "Multi-body motion modeling and simulation for tilt rotor aircraft," *Chin. J. Aeronaut.*, vol. 23, no. 4, pp. 422–425, 2010.
[20] F. Zhang, L. U. Ping, T. Jiang, and F. M. Shi, "Transitional mode manipulation strategy of tilt tri-rotor UAVs based on fuzzy control," *Electron. Opt. Control*, vol. 25, no. 4, pp. 32–36, 2018.
[21] X. Yan and R. Chen, "Augmented flight dynamics model for pilot workload evaluation in tilt-rotor aircraft optimal landing procedure after one engine failure," *Chin. J. Aeronaut.*, vol. 32, no. 1, pp. 92–103, Jan. 2019.
[22] T. Wang, J. Wang, C. Wu, M. Zhao, and T. Ge, "Disturbance-rejection control for the hover and transition modes of a negative-buoyancy quad tilt-rotor autonomous underwater vehicle," *Appl. Sci.*, vol. 8, no. 12, p. 2459, Dec. 2018.
[23] N. K. Rout, D. P. Das, and G. Panda, "PSO based adaptive narrowband ANC algorithm without the use of synchronization signal and secondary path estimate," *IEEE Access*, vol. 7, pp. 18840–18859, 2019.
[24] Z. Yin, C. Du, J. Liu, X. Sun, and Y. Zhong, "Research on autodisturbance-rejection control of induction motors based on an ant colony optimization algorithm," *IEEE Trans. Ind. Electron.*, vol. 65, no. 4, pp. 3077–3094, Apr. 2018.
[25] G. Wang, J. Guo, Y. Chen, Y. Li, and Q. Xu, "A PSO and BFO-based learning strategy applied to faster R-CNN for object detection in autonomous driving," *IEEE Access*, vol. 7, pp. 18840–18859, 2019.
[26] B. C. Mohan and R. Baskaran, "A survey: Ant colony optimization based recent research and implementation on several engineering domain," *Expert Syst. Appl.*, vol. 39, no. 4, pp. 4618–4627, Mar. 2012. [Online]. Available: http://www.sciencedirect.com/science/article/pii/S0957417411013996
[27] S. Gao, Y. Wang, and J. Cheng, "Ant colony optimization with clustering for solving the dynamic location routing problem," *Appl. Math. Comput.*, vol. 285, pp. 149–173, Jul. 2016.
[28] C. Lin, H. Wang, J. Yuan, and M. Fu, "An online path planning method based on hybrid quantum ant colony optimization for AUV," *Int. J. Robot. Autom.*, vol. 33, no. 4, pp. 435–444, 2018.
[29] J. Li, B. Xu, Y. Yang, and H. Wu, "Three-phase qubits-based quantum ant colony optimization algorithm for path planning of automated guided vehicles," *Int. J. Robot. Autom.*, vol. 34, no. 2, pp. 156–163, 2019.
[30] L. Wang, C. Luo, M. Li, and J. Cai, "Trajectory planning of an autonomous mobile robot by evolving ant colony system," *Int. J. Robot. Autom.*, vol. 32, no. 4, pp. 406–413, 2017.
[31] Z. Lu and H. Wang, "An event-based supply chain partnership integration using a hybrid particle swarm optimization and ant colony optimization approach," *Appl. Sci.*, vol. 10, no. 1, p. 190, Dec. 2019.
[32] L. V. Tran, B. H. Huynh, and H. Akhtar, "Ant colony optimization algorithm for maintenance, repair and overhaul scheduling optimization in the context of industrie 4.0," *Appl. Sci.*, vol. 9, no. 22, p. 4815, Nov. 2019.
[33] E. Oh and H. Lee, "Development of a convolution-based multi-directional and parallel ant colony algorithm considering a network with dynamic topology changes," *Appl. Sci.*, vol. 9, no. 18, p. 3646, Sep. 2019.
[34] M. Schlüter, J. A. Egea, L. T. Antelo, A. A. Alonso, and J. R. Banga, "An extended ant colony optimization algorithm for integrated process and control system design," *Ind. Eng. Chem. Res.*, vol. 48, no. 14, pp. 6723–6738, Jul. 2009.
[35] N. Zhang, Z.-R. Feng, and L.-J. Ke, "Guidance-solution based ant colony optimization for satellite control resource scheduling problem," *Int. J. Speech Technol.*, vol. 35, no. 3, pp. 436–444, Dec. 2011.
[36] Q. Geng and P. Tian, "The ADRC design for UAV longitudinal channel and its parameter optimization based on ACO," in *Proc. IEEE Int. Conf. Control Autom.*, Jun. 2013, pp. 373–377.
[37] S. Gao, M. Zhou, Y. Wang, J. Cheng, H. Yachi, and J. Wang, "Dendritic neuron model with effective learning algorithms for classification, approximation, and prediction," *IEEE Trans. Neural Netw. Learn. Syst.*, vol. 30, no. 2, pp. 601–614, Feb. 2019.

ZHICHAO LYU received the B.Sc. degree in optical fiber communications from the Chongqing University of Posts and Telecommunications, Chongqing, China, in 2012, and the M.Sc. degree in aerospace engineering from the Harbin Institute of Technology, Harbin, China, in 2015. From 2015 to 2019, she worked as an Engineer with the Hongdu Aircraft Design Institute of AVIC. Since 2020, she has been an Engineer with the Yangzhou Collaborative Innovation Research Institute. Her research interests include top-level design, scheme design, POP, ICD, detail design of avionics system, UAV bee colonies, UAV obstacle avoidance technology, and manned and UAV coordinated operations.

ZHIGANG WANG received the B.Sc. degree in space science and technology and the M.Sc. degree in software engineering from the Harbin Institute of Technology, Harbin, China, in 2012 and 2014, respectively, and the Ph.D. degree in aerospace vehicle design from the Nanjing University of Aeronautics and Astronautics, Nanjing, China, in 2020. He currently works as an Engineer with the Yangzhou Collaborative Innovation Research Institute. His research interests include dynamic modeling and control of novel aircraft, intelligent optimization algorithm, navigation and obstacle avoidance of aircraft in denial environment, and cooperative control of swarm formation.

DENGYAN DUAN received the B.Sc. degree in aerospace vehicle design from the Nanjing University of Aeronautics and Astronautics, Nanjing, China, in 2017, where she is currently pursuing the Ph.D. degree. Her research interests include aerodynamic and dynamic modeling and control of novel aircraft, collaborative formation, and so on.

LILI LIN received the B.Sc. degree in aircraft design engineering from Nanchang Hangkong University, Nanchang, China, in 2017, and the M.Sc. degree in aviation engineering from the Nanjing University of Aeronautics and Astronautics, Nanjing, China, in 2020. He currently works as an Engineer with the Yangzhou Collaborative Innovation Research Academy. His research interests include conceptual design of plane and new concept rotorcraft.

JIANBO LI is currently a Researcher and a Ph.D. Supervisor with the Key Laboratory of Helicopter Rotor Dynamics for National Defense Science and Technology, Nanjing University of Aeronautics and Astronautics. He is Jiangsu Province 333 High-level Talent Training Project Young and Middle-aged Scientific and Technological Leaders and 321 Science and Technology Leading Talents. His main research interests include overall design of rotor aircraft and the integrated design of unmanned helicopter systems.

YONGWEN YANG received the Bachelor of Engineering and the Master of Aircraft Design degrees from the Nanjing University of Aeronautics and Astronautics, in 2006 and 2011, respectively. He is currently working with Yangzhou Collaborative Innovation Research Institute Company Ltd. He is also a Senior Engineer. His main research interests include new concept aircraft market and demand analysis and overall scheme design.

YONGHONG CHEN received the Ph.D. degree from the Shenyang Institute of Automation, Chinese Academy of Sciences. She currently works as the Vice Minister and a Chief Project Designer with Yangzhou Collaborative Innovation Research Institute Company Ltd. She is also a Senior Engineer. Her research interests include collaborative operations and integrated design of radio frequency systems.

YIBO LI received the Ph.D. degree in aircraft design from the Beijing University of Aeronautics and Astronautics, Beijing, China, in 2012. He is currently the Deputy General Manager and a Technical Director of the Yangzhou Collaborative Innovation Research Institute Company Ltd. He is also a Researcher. His research interest includes overall design of the novel aircraft.